



**HAL**  
open science

## A highly selective FER-based catalyst to produce n-butenes from isobutanol

Stijn van Daele, Delphine Minoux, Nikolai Nesterenko, Sylvie Maury, Vincent Coupard, Valentin Valtchev, Arnaud Travert, Jean-Pierre Gilson

► **To cite this version:**

Stijn van Daele, Delphine Minoux, Nikolai Nesterenko, Sylvie Maury, Vincent Coupard, et al.. A highly selective FER-based catalyst to produce n-butenes from isobutanol. *Applied Catalysis B: Environmental*, 2021, 284, pp.119699. 10.1016/j.apcatb.2020.119699 . hal-03035180

**HAL Id: hal-03035180**

**<https://normandie-univ.hal.science/hal-03035180>**

Submitted on 2 Dec 2020

**HAL** is a multi-disciplinary open access archive for the deposit and dissemination of scientific research documents, whether they are published or not. The documents may come from teaching and research institutions in France or abroad, or from public or private research centers.

L'archive ouverte pluridisciplinaire **HAL**, est destinée au dépôt et à la diffusion de documents scientifiques de niveau recherche, publiés ou non, émanant des établissements d'enseignement et de recherche français ou étrangers, des laboratoires publics ou privés.

# Journal Pre-proof

A highly selective FER-based catalyst to produce n-butenes from isobutanol

Stijn Van Daele (Conceptualization) (Data curation) (Investigation) (Software) (Validation) (Formal analysis) (Writing - original draft) (Writing - review and editing), Delphine Minoux (Conceptualization) (Supervision), Nikolai Nesterenko (Conceptualization) (Funding acquisition) (Project administration) (Supervision) (Writing - review and editing), Sylvie Maury (Conceptualization) (Writing - review and editing), Vincent Coupard (Conceptualization) (Writing - review and editing), Valentin Valtchev (Conceptualization) (Writing - original draft) (Writing - review and editing), Arnaud Travert (Conceptualization) (Data curation) (Formal analysis) (Investigation) (Software) (Validation) (Writing - original draft) (Writing - review and editing), Jean-Pierre Gilson (Conceptualization) (Funding acquisition) (Project administration) (Writing - original draft) (Writing - review and editing)



PII: S0926-3373(20)31116-4  
DOI: <https://doi.org/10.1016/j.apcatb.2020.119699>  
Reference: APCATB 119699

To appear in: *Applied Catalysis B: Environmental*

Received Date: 23 July 2020  
Revised Date: 23 October 2020  
Accepted Date: 24 October 2020

Please cite this article as: Van Daele S, Minoux D, Nesterenko N, Maury S, Coupard V, Valtchev V, Travert A, Gilson J-Pierre, A highly selective FER-based catalyst to produce n-butenes from isobutanol, *Applied Catalysis B: Environmental* (2020), doi: <https://doi.org/10.1016/j.apcatb.2020.119699>

This is a PDF file of an article that has undergone enhancements after acceptance, such as the addition of a cover page and metadata, and formatting for readability, but it is not yet the definitive version of record. This version will undergo additional copyediting, typesetting and review before it is published in its final form, but we are providing this version to give early visibility of the article. Please note that, during the production process, errors may be discovered which could affect the content, and all legal disclaimers that apply to the journal pertain.

© 2020 Published by Elsevier.

# A highly selective FER-based catalyst to produce n-butenes from isobutanol

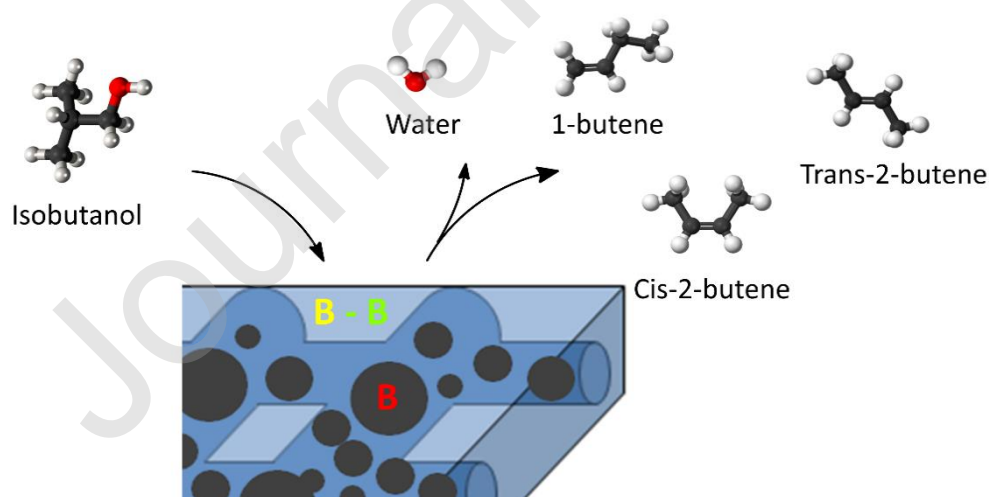
*Stijn Van Daele<sup>a,b</sup>, Delphine Minoux<sup>b</sup>, Nikolai Nesterenko<sup>b</sup>, Sylvie Maury<sup>c</sup>, Vincent Coupard<sup>c</sup>, Valentin Valtchev<sup>a</sup>, Arnaud Travert<sup>a\*</sup> and Jean-Pierre Gilson<sup>a</sup>*

a) Normandie Univ, ENSICAEN, UNICAEN, CNRS, LCS, 14000 Caen, France

b) Total Research and Technology Feluy (TRTF), Zone Industrielle C, 7181 Feluy, Belgium

c) IFPEN, Rond-point de l'échangeur de Solaize, 69360 Solaize, France

\* [arnaud.travert@ensicaen.fr](mailto:arnaud.travert@ensicaen.fr)



**Graphic for TOC** Selective n-butenes production from isobutanol – (cascade) reaction scheme.

### Highlights

- The use of FER as catalyst for the dehydration of iso-butanol results in an excellent selectivity for n-butenes
- The external Brønsted acid sites function as isobutanol dehydration active sites
- High external Brønsted acidity improves selectivity to n-butenes
- Use of *in-situ* and *operando* characterisation toolboxes allowed identifying the active sites.

The conversion of isobutanol to light olefins over zeolites was investigated by IR *operando* spectroscopy. FER zeolites showed a surprisingly high selectivity for the direct conversion of iso-butanol to linear butenes, hence catalyzing dehydration and skeletal isomerization in one step. As a fundamental understanding of the separate reactions is required to design superior catalysts, an *in-situ* and *operando* FT-IR mechanistic study of the reaction was carried out. The spectroscopic data, the derived species participating and their respective role are analyzed using chemometric (PCA and MCR-ALS) tools. We highlighted the role played by the external acid sites and the requirement of a specific distance between these sites to ensure the n-butene selectivity and point that the internal Brønsted acidity has an adverse effect on the catalyst stability. Moreover, there is no correlation between the carbon species formed on the surface and the exceptional selectivity towards n-butenes, allowing to exclude a “carbon pool” mechanism.

**Keywords:** isobutanol, linear butenes, zeolite, Ferrierite, *operando* FT-IR, chemometrics, MCR-ALS

## Introduction

The search for sustainable pathways to the major building blocks of the petrochemical industry is a lively research topic. The adverse effects of climate change, a C<sub>4</sub>-shortage and recent progress in bio-chemical isobutanol synthesis made isobutanol an attractive fuel component and platform molecule for petrochemistry.[1–3] Its dehydration provides a renewable source of C<sub>4</sub> molecules, precursors of higher value products such as butyl rubber (automotive market), polyisobutylene (lubricant), and ethyl tert-butyl ether (fuel additive).

The dehydration of butanol isomers is a well-established reaction catalyzed by many solid acids, such as  $\gamma$ -alumina. Generally, the isomer produced at low temperatures (< 673 K) is the direct dehydration product.[4–6] Moreover, isobutene is thermodynamically favored over linear butenes (see e.g. ref. [7] and Table S1 of the SI) and generally prevails during the isobutanol dehydration as it is often both the kinetic and thermodynamic product. When the dehydration is accompanied by simultaneous or consecutive skeletal isomerization, the selectivity to linear butene isomers is altered.[8,9] Such a cascade reaction produces all linear butene isomers, regardless of the initial butanol isomer used as a reactant. However, when using a  $\gamma$ -alumina catalyst, the second step is slow and requires high contact times, therefore, limiting its industrial interest for linear butene production.[10]

More recently, a technology for isobutanol dehydration to linear butenes, ATOL-C<sub>4</sub><sup>TM</sup> was developed in a joint collaboration between IFPEN, Total Research & Technology Feluy and Axens. The dehydration reaction takes place in the gas phase with a low water dilution of the alcohol feedstock in a fixed-bed multi-tubular reactor on a ferrierite (FER)-based catalyst.[11] The process is very attractive since in this case the isobutanol conversion is almost complete in a single pass, the reaction-regeneration cycles enable to maintain the catalyst performances for several months, and the selectivity to linear butenes is very high.

However, an improved fundamental understanding of the separate reactions (dehydration and isomerization) is required to design even better performing catalysts. Extensive research on the skeletal isomerization of 1-butene to isobutene started more than two decades ago and highlighted the high activity and selectivity of zeolites with medium pore openings (10 MR: FER- and TON-type). [12–16] Although some details are still debated, it is generally accepted that both mono- and bimolecular mechanisms occur on the fresh catalyst, while the monomolecular prevails on an aged catalyst. Moreover, the participation of carbonaceous species, formed at the pore mouths/external surface of the zeolite, was proposed in a pseudo-monomolecular reaction mechanism. This led Zhang *et al.* to use Ferrierite for the one-step conversion of *n*-butanol to isobutene between 673 - 773 K.[10] . However, they concluded that Ferrierite is not stable under these operating conditions as its framework is dealuminated.

This study explores the direct conversion of isobutanol into *n*-butenes on Ferrierite, a cascade reaction where isobutanol dehydration is followed by the skeletal isomerization of the primary products, at low temperature (< 573 K) to alleviate the deactivation.[11,17,18] We focus in particular on the fine-tuning of the acidic and textural properties of Ferrierite and use IR *operando* spectroscopy to gain more insight into the global reaction mechanism. Due to the complex nature of such IR spectra, spectral interpretations are assisted by chemometric tools to provide relevant information on the surface species, including those leading to deactivation. Our study highlights an unexpectedly high *n*-butenes selectivity, shed some light on the reaction mechanism, and relates performance with structural and textural features of the FER-type zeolite.

## Materials and methods

### *Samples*

Commercial ferrierites (CP 914C and CP 914) were supplied by Zeolyst International and hereinafter referred to as FER $x$  ( $x$ =Si/Al molar ratio), namely FER9 and FER28. FER28 was used as the reference unless otherwise specified. A third home-made sample, FER46 was evaluated. Two other samples were prepared according to recently published reports [19,20]; both are nanosized crystals with different morphologies, namely needle and plate-like ferrierites (respectively FER NN and FER NP). These two samples are referred to in graphs as FER Nano. Both MFI and gamma-alumina were commercial samples provided by Zeolyst International (CBV 8014) and Sigma-Aldrich, respectively. An ERI (Erionite) and a TON zeolite (ZSM-22) were prepared according to published procedures.[21] The ammonium form of the zeolites was converted to their protonic form by calcination at 773 K for 5 h, (ramp rate of 1 K min<sup>-1</sup> under dry air flow). Table 1 summarizes an overview of all characterization results of the samples, which will be reported upon later in this work.

### *Post-synthetic modifications*

#### Na-exchanged zeolites

To evaluate the influence of the number of acid sites on the reaction, the ammonium forms of the zeolites were partially ion-exchanged with sodium. Sodium nitrate solutions of different concentrations (0.1 M, 0.01 M, 0.001 M) were mixed with the zeolites (1 g zeolite / 25 mL solution) at 353 K for 10, 60 and 180 min, filtered and washed with distilled water prior to collecting the zeolite. The process was repeated one to three times to achieve a wide range of ion-exchange (40-96 %). The samples were then dried overnight at 373 K prior to calcination (*vide supra*). The percentage of sodium introduced was determined by *in-situ* FT-IR of deuterated acetonitrile. These samples are referred to in graphs as FER Na.

#### Modification of the external acidity

The external surface of the FER zeolite was passivated according to the procedure reported by Losch *et al.*[22] - 0.5 g of zeolite was suspended in 12.5 mL of *n*-hexane (Sigma-Aldrich > 99 % purity) and refluxed at 353 K under vigorous stirring (500 rpm). Next, 0.150 mL TEOS (4 wt. % of SiO<sub>2</sub> with respect to the parent zeolite) was added, and the mixture stirred for 1 h. The *n*-hexane was then removed by evaporation, and the zeolite calcined at 823 K for 4 h (FER 1SP). This procedure was repeated twice to ensure complete surface coverage (FER 2SP). The ratio of Brønsted/Lewis acidity on the external surface was adjusted by aluminum chemical deposition with aluminum isopropoxide (Al(O-*i*Pr)<sub>3</sub>). A procedure similar to the surface silylation was developed, albeit with a lower amount, 1.5 wt. % of aluminum, to avoid clustering of the Lewis acid sites (FER ESA). These three samples are referred to in graphs as FER SP (SP stands for surface passivation).

### Steaming

FER28 was first calcined under air (dry air flow, 25 cc min<sup>-1</sup>) at 723 K (ramp rate of 1 K min<sup>-1</sup>) for 6 hours prior to steaming (523, 623 and 823 K for 4 hours under a 20 vol. % H<sub>2</sub>O / N<sub>2</sub> flow, 25 cc min<sup>-1</sup>) and cooling down to room temperature under a flow of dry N<sub>2</sub> (25 cc min<sup>-1</sup>). These three samples are referred to in graphs as FER steamed.

### Catalyst characterization

A Micromeritics 2020 ASAP was used for nitrogen sorption measurements. The samples were first outgassed at 373 K for 1 h and 623 K for 10 h prior measurements. Scanning Electron Microscopy (SEM) pictures were recorded on a Tescan (MIRA/LMH) microscope equipped with a field emission gun. The nanometer-sized zeolites were further characterized by Transmission Electron Microscopy (TEM) on a Philips CM 120 microscope equipped with a LaB<sub>6</sub> filament. The catalysts regeneration by combustion of the carbonaceous residue

(“coke”) was monitored with a Setaram SDT Q600 TA thermogravimetric analyzer coupled by heating up to 1173 K ( $5 \text{ K min}^{-1}$ ) under a  $100 \text{ ml min}^{-1}$  (10 %  $\text{O}_2$  in He) flow.

Solid-state magic angle spinning nuclear magnetic resonance spectroscopy (MAS-NMR) was used to characterize the local  $^{27}\text{Al}$  environments in the zeolite samples. All data were recorded on a Bruker Advance III - 500 MHz spectrometer using 4 mm rotors. The  $^{27}\text{Al}$  MAS NMR spectra were recorded at 130.29 MHz with a p/12 pulse length of 0.77 ns, a spinning rate of 14 kHz and a recycle delay of 1 s.  $\text{Al}(\text{NO}_3)_3$  (1 M) was used as a reference for chemical shifts for  $^{27}\text{Al}$ . Samples were left overnight in a desiccator with a saturated NaCl salt solution to ensure an equilibrated and steady water content.  $\{^1\text{H}\}$ - $^{13}\text{C}$  cross-polarization (CP) MAS experiments were performed using a spinning frequency of 12 kHz. A contact time of 1.5 ms and a recycle time of 2 s were used. The number of scans was varied between 5000 and 60000 depending on the amount of carbon remaining after regeneration. Tetramethylsilane (TMS) was selected as reference to measure  $^{13}\text{C}$  chemical shifts.

*In-situ* FT-IR spectroscopy was used to quantify the acidity of the zeolites on a Nicolet Magna 550-FTIR spectrometer at  $4 \text{ cm}^{-1}$  optical resolution equipped with a DTGS detector. The samples were pressed under 1 ton into self-supported wafers (diameter  $2 \text{ cm}^2$ , 18 mg) prior to loading in the IR cell. Before spectra acquisition (298 K), each sample was activated in the IR cell connected to a vacuum line (393 K reached at  $1 \text{ K min}^{-1}$  for 4 h followed by 5 h at 723 K reached at  $1 \text{ K min}^{-1}$  under a vacuum of  $10^{-6}$  torr). Perdeuterated acetonitrile was used to quantify the total acidity and its nature (Brønsted/Lewis) as this molecule probes both the 8- and 10-membered rings of the FER porosity.[15,23] 2,6-dimethyl pyridine and *tert*-butyl nitrile were used to quantify respectively the Brønsted and Lewis acid sites located on the external crystal surface.[24,25] *n*-hexane ( $4.3 \text{ \AA}$ ), too bulky to reach the 8 MR cavities ( $3.5 \times 4.8 \text{ \AA}$ ), was selected to quantify the Brønsted acidity in the 10 MR ( $4.5 \times 5.4 \text{ \AA}$ )

channels [26,27] (see Figure S1 of the SI). All probe molecules were adsorbed at ambient temperature (295 K) and an equilibrium pressure of 0.5 torr. Difference spectra were reported by subtracting a reference spectrum (recorded after activation and prior to adsorption of any probe molecule) from the spectra of interest. The characteristics of all samples investigated are summarized in Table 1.

### *Catalytic tests*

The catalytic performances were evaluated in a fixed-bed plug-flow reactor (PFR) at 523 K under conditions free from external diffusion limitation (see Figure S2 of the SI). The zeolite powders were pressed, crushed and sieved to a size between 100 and 200  $\mu\text{m}$  and diluted in silicon carbide (100 - 200  $\mu\text{m}$  and a Zeolite/SiC<sub>4</sub> ratio of 1/20) to obtain a 1 cm reactor bed height. The powders were activated in the reactor at 393 K (1 K min<sup>-1</sup>) for 4 h, the temperature raised to 723 K (1 K min<sup>-1</sup>) and kept for 5 h under a 25 cc min<sup>-1</sup> flow of lean air (95 % N<sub>2</sub> - 5 % O<sub>2</sub>) before cooling to the reaction temperature. Trans-2-butene and isobutene, (Air Liquid) were continuously fed to the reactor using mass flow controllers, while a saturator was used to supply isobutanol (Sigma Aldrich) vapors. The reaction products were analyzed online with a Bruker 450 gas chromatograph fitted with an FID and a Thermo TG-bond Q capillary column. The reaction rates are reported as pseudo-first order rate constants  $k$ , calculated from the following formula:

$$k = \frac{F}{W} \ln \frac{1}{1 - X_{t=4h}}$$

where  $W$  is the catalyst mass (g),  $F$  is the reactant flow rate ( $\mu\text{mol min}^{-1}$ ) and  $X_{t=4h}$  is the fractional conversion after four hours on stream.

The  $n$ -butene selectivities were interpolated to the same conversion (50 %, standard deviation of 0.8 %, Figure S3 of the SI) and collected after 4 h time-on-stream. The octenes

selectivities were calculated by interpolating the sum of the octenes and its cracking product, propene, to the same conversion (50 %, standard deviation of 0.3 %).

#### *Operando* IR measurements

The transmission *operando* IR cell, its validation and use were reported earlier by Li *et al.*[28] To avoid external diffusion limitations, a self-supporting wafer with a surface of 2 cm<sup>2</sup> obtained by pressing a mixture of approximately 5 mg of zeolite and 15 mg of inert silica was loaded in the reactor and activated as discussed above. The IR measurements were carried out on a Nicolet 6700 FT-IR instrument equipped with an MCT detector at 4 cm<sup>-1</sup> resolution. After activation, a spectrum of the clean sample was recorded and used as the reference, subtracted from the spectra recorded during the reaction. These resulting difference spectra were corrected for the water present in the gas phase and in the optical path. After reaction, the reactant flow was stopped and a spectrum recorded after a 20 minutes nitrogen purge.

#### *Chemometrics*

The chemometric analysis was performed with SpectroChemPy, a python API.[29][30] The Multivariate-Curve Regression by Alternating Least Squares (MCR-ALS) algorithm was selected to extract more information on the nature of the species reacting on the surface of the catalysts and their kinetics.[31] A Principal Component Analysis (PCA) was first used to determine the optimum number of pure species to adequately describe the experimental spectra  $X$ . Once the number of principal components was known, a first estimate of the concentration profile  $C$  of these species was calculated via an Evolving Factor Analysis

(EFA) algorithm. The spectra and concentration profile of pure species could then be estimated from the matrix of experimental spectra ( $X$ ) by solving the linear matrix equation:

$$X = C S^T + E$$

Where  $C$  is the MCR-ALS concentration profile (dimensionless),  $S^T$  is the matrix of spectral profiles (absorbance units) and  $E$  the matrix of residuals (absorbance units) unaccounted by the model. These concentration and spectral profiles were further optimized by an alternate least square algorithm (MCR-ALS), including hard constraints such as the non-negativity of concentration and spectral profiles, as reported by Vilmin *et al.*[32] Our MCR-ALS optimization was performed on a limited spectral region, 1700 – 1300  $\text{cm}^{-1}$ , allowing to impose the non-negativity of spectral profiles and improve the optimization robustness. We assumed that the concentration profile  $C_{1700-1300}$  for this region provided sufficient information to reconstruct the whole spectral region. The validity of this hypothesis was tested by comparing the original spectra with the reconstructed dataset  $\hat{X} = C S^T$ . The global algorithm is summarized in Table S2, which can be found in the supporting information

Table 1. Physicochemical characteristics of the employed Ferrierite samples.

Catalyst	<u>parents FER</u>			<u>Steamed FER28</u>			<u>Surface modified FER28</u>		
	FER 9	FER 28	FER 46	523 K	623 K	823 K	1x TEOS	2x TEOS	1 x Al(O- iPr) <sub>3</sub>
Si/Al	9	28	46	28	28	28	28	28	28
V <sub>micro</sub> (cm <sup>3</sup> /g)	0.15	0.14	0.10	0.13	0.13	0.13	0.12	0.12	0.13
S <sub>ext</sub> (m <sup>2</sup> g <sup>-1</sup> )	25	18	14	46	46	48	42	39	44
B <sub>tot</sub> - L <sub>tot</sub> (μmol g <sup>-1</sup> )	770 - 795	540 - 70	307 - 30	580 - 46	570 - 69	420 - 142	530 - 82	460 - 96	550 - 89
B <sub>10MR</sub> / B <sub>tot</sub> (%)	16	53	56	48	56	51	51	50	49
B <sub>ext</sub> - L <sub>ext</sub> (μmol g <sup>-1</sup> )	26 - 6	17 - 11	16 - 0	13 - 12	8 - 11	7 - 5	12 - 6	5 - 1	13 - 19
k (mol h <sup>-1</sup> g <sub>cat</sub> <sup>-1</sup> )	3.13	1.50	1.57	1.36	0.95	0.61	0.70	0.37	0.68
S <sub>n-C4</sub> (%)	80.4	81.4	85.0	80.2	81.0	81.2	76.3	74.7	76.8

Catalyst	FER28	<u>Partial Na exchange</u>				<u>Spent</u>	<u>Nanosized samples</u>	
		30 % Na	60 % Na	86 % Na	96 % Na		Nanoneedle	Nanoplate
Si/Al	28	28	28	28	28	28	14	9
$V_{\text{micro}}$ (cm <sup>3</sup> /g)	0.14	0.13	0.13	0.13	0.13	0.0004	0.10	0.13
$S_{\text{ext}}$ (m <sup>2</sup> g <sup>-1</sup> )	18	50	42	38	40	37	240	42
$B_{\text{tot}} - L_{\text{tot}}$ (μmol g <sup>-1</sup> )	540 - 70	380 - 57	220 - 42	75 - 48	22 - 53	64 - 4	688 - 275	697 - 937
$B_{10\text{MR}} / B_{\text{tot}}$ (%)	53	75	98	88	100	9	5	28
$B_{\text{ext}} - L_{\text{ext}}$ (μmol g <sup>-1</sup> )	17 - 11	15 - 11	16 - 14	18 - 11	17 - 14	7 - 4	36 - 85	17 - 13
$k$ (mol h <sup>-1</sup> g <sub>cat</sub> <sup>-1</sup> )	1.50	1.48	1.24	1.12	1.00	0.34	5.21	3.99
$S_{\text{n-C4}}$ (%)	81.4	80.6	79	80.7	80.8	70.8	75.4	84.1

## Results and discussion

### *Preliminary catalyst screening*

Five catalysts including  $\gamma$ -Al<sub>2</sub>O<sub>3</sub> and four zeolites of different structures (ERI, FER, TON, and MFI) were first evaluated in the conversion of isobutanol (Table 2). Both activity and n-butene selectivity of all zeolites are significantly higher than those of  $\gamma$ -alumina, suggesting that confinement in the zeolite porosity or strong Brønsted acidity promotes n-butene selectivity.

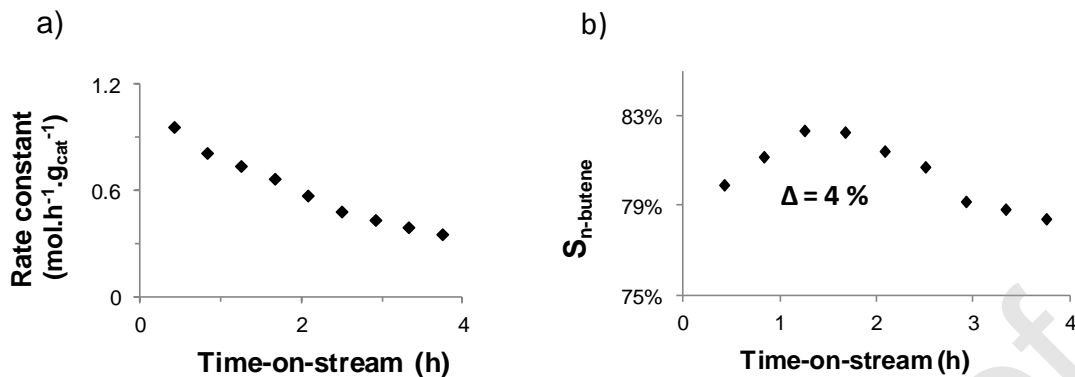
Among the zeolites, Ferrierite (FER28) displays an excellent activity and the highest n-butenes selectivity (81.4 % at 50 % conversion), confirming earlier results.[17] It is worth noticing that such a ranking seems paradoxical as the FER-type zeolite is well-known to efficiently catalyze the skeletal isomerization of n-butene to iso-butene.[33] Table S1 (SI) compares the experimental distribution of butene isomers with their thermodynamic equilibrium and shows that the experimental ratio of linear butenes to isobutene (4.89) is much larger than at thermodynamic equilibrium (0.70). On the other hand, the internal distribution between linear butenes is close to thermodynamic equilibrium. This suggests that isobutene and linear butenes are formed from distinct routes and that thermodynamic equilibrium is rapidly reached between the linear butenes. Finally, it is worth pointing out that at our conditions isobutanol dehydration to butenes is not thermodynamically limited.

Table 2. Characteristics and performances of catalysts in one-step isobutanol transformation

Catalyst	$\gamma$ -alumina	ERI4	FER28	TON36	MFI40
Si/Al	-	4	28	36	40
$V_{\text{micro}}^{\text{a}}$ (cm <sup>3</sup> /g)	0.08	0.19	0.14	0.11	0.10
$S_{\text{ext}}^{\text{a}}$ (m <sup>2</sup> g <sup>-1</sup> )	208	69	18	70	100
$k$ (mol h <sup>-1</sup> g <sub>cat</sub> <sup>-1</sup> )	0.08	0.33	1.50	2.08	1.97
$S_{\text{n-C4}}^{\text{b}}$ (%)	1.36	30.5	81.4	62.1	23.3

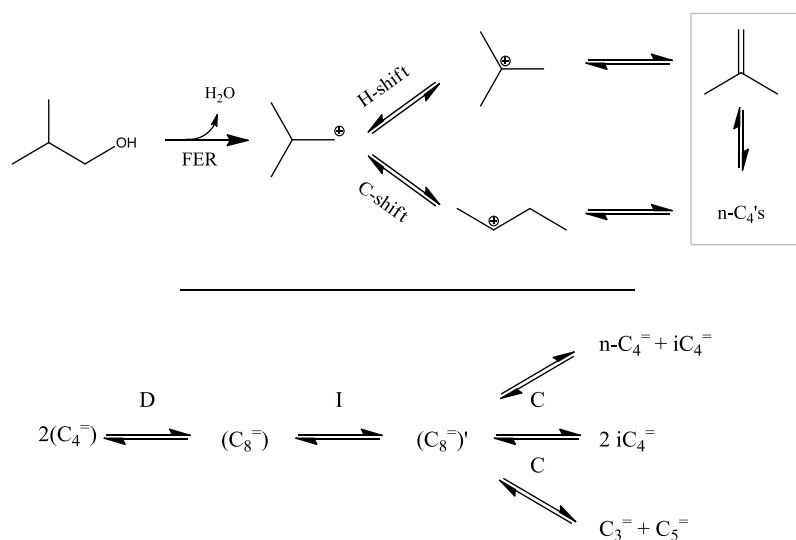
(<sup>a</sup> t-plot, <sup>b</sup> at 50 % conversion, reaction conditions: T = 523 K, WHSV = 100 h<sup>-1</sup>, P<sub>atm</sub> = 1 bar, P<sub>isobutanol</sub> = 45 mbar, TOS = 4 h)

Figure 1a shows the evolution of the reaction rate constant on FER28 with time on stream and indicates a continuous deactivation; this could be the result of acid site poisoning or pore plugging. The deactivation is accompanied by a change of the n-butene selectivity showing a maximum after approximately two hours. It is worth noting that such a change (+ 4 %) remains small and is not as pronounced as those reported for 1-butene to isobutene isomerization (typically ~ 40 % increase with time on stream).[34] Because of the similarities between the two reactions, however, such selectivity change deserves further investigation.



**Figure 1.** Evolution of (a) the pseudo-first order rate constant, (b) n-butene selectivity with time-on-stream (h) for FER28. (reaction conditions: *operando* reactor, T = 525 K, WHSV = 100 h<sup>-1</sup>, P<sub>atm</sub> = 1 bar, P<sub>isobutanol</sub> = 45 mbar, TOS = 4 h)

Minor amounts of side products (propene, pentenes and octenes) were also formed. Figure 2 illustrates the possible reaction pathways for the reaction. Butenes are the major products together with some propene, pentenes and octenes. *n*-butenes are either primary products or secondary products obtained by isobutene isomerization. As shown in the bottom of Figure 2, Minor products are probably formed by butene dimerization followed by cracking to propene and pentenes.[35,36]



**Figure 2.** Top: dehydration and isomerization of isobutanol on FER, Bottom: Side products formation starting with butene dimerization (D), followed by isomerization (I) and cracking (C) of the resulting octenes [37]

### *Influence of Si/Al ratio*

Three FER-type zeolites with increasing Si/Al (9, 28 and 46), FER9, FER28, FER46 have been compared in the conversion of isobutanol to *n*-butenes; their characteristics, catalytic activities (pseudo first-order rate constants) and *n*-butene selectivities are gathered in Table 3 and Table 4. While FER28 and FER46 are similar but for their Si/Al, FER9 differs by a high Lewis/Brønsted acidity ratio and a low fraction of Brønsted acid sites in its 10 MR channel. FER9 displays the highest pseudo-first order rate constant while FER46 is the most selective towards *n*-butene. However, no correlation was found between the aluminum content and the dehydration rate constant or *n*-butene selectivity. Increasing the aluminum content leads to an

increased total Lewis acidity, as shown by *in-situ* IR ( $795 > 70 > 30 \mu\text{mol g}^{-1}$  for FER9, FER28 and FER46, respectively). On the other side, the Lewis acidity of the external surface does not increase proportionally with the total aluminum content. Moreover, the catalytic results on FER46 show that the absence of Lewis acidity on the external surface has no impact on the dehydration rate and *n*-butene selectivity. This finding suggests that the external Lewis acidity does not play an essential role in the reaction. On the other hand, the high activity of FER9 appears to be correlated with the external Brønsted acid sites density: the latter is twice as high as the other FER zeolites and its activity is also doubled.

**Table 3.** Characteristics of FER catalysts with different Si/Al ratios

Catalyst	FER9	FER28	FER46
Commercial name	CP 914C	CP 914	-
$B_{\text{tot}} - L_{\text{tot}}$ ( $\mu\text{mol g}^{-1}$ )	770 - 795	540 - 70	307 - 30
$B_{10\text{MR}} / B_{\text{tot}}$ (%)	16	53	56
$B_{\text{ext}} - L_{\text{ext}}$ ( $\mu\text{mol g}^{-1}$ )	26 - 6	17 - 11	16 - 0
$k$ ( $\text{mol h}^{-1} \text{g}_{\text{cat}}^{-1}$ )	3.13	1.50	1.57
$S_{\text{n-C}_4}$ <sup>a</sup> (%)	80.4	81.4	85.0

(<sup>a</sup> at 50 % isobutanol conversion in a tubular PFR, reaction conditions:  $T = 523 \text{ K}$ ,  $\text{WHSV} = 100 \text{ h}^{-1}$ ,  $P_{\text{atm}} = 1 \text{ bar}$ ,  $P_{\text{isobutanol}} = 45 \text{ mbar}$ ,  $\text{TOS} = 4 \text{ h}$ )

**Table 4.** Isobutanol dehydration/isomerization on FER zeolites

Catalyst	Yields (%)					Ratio (%)	Selectivity (%)
	$i\text{-C}_4^{\text{=}}$	$n\text{-C}_4^{\text{=}}$	$\text{C}_3^{\text{=}}$	$\text{C}_5^{\text{=}}$	$\text{C}_8^{\text{=}}$	$i\text{-C}_4^{\text{=}}/\text{total C}_4^{\text{=}}$	$n\text{-C}_4^{\text{=}}$
FER9	9.1	38.2	0.1	0.0	0.1	19.1	80.4
FER28	4.3	17.5	0.1	0.0	0.2	20.0	81.4
FER46	5.6	28.8	0.1	0.0	0.1	15.9	85.0

(<sup>a</sup> at 50 % isobutanol conversion in a tubular PFR, reaction conditions:  $T = 523 \text{ K}$ ,  $\text{WHSV} = 100 \text{ h}^{-1}$ ,  $P_{\text{atm}} = 1 \text{ bar}$ ,  $P_{\text{isobutanol}} = 45 \text{ mbar}$ ,  $\text{TOS} = 4 \text{ h}$ )

#### *Impact of water on the catalyst structure and activity*

As water is formed during the reaction, its potential impact on the stability of the FER catalysts needs to be investigated. To this end, the reference sample (FER28) is steamed *ex-situ* at three different temperatures: two near the reaction temperature (523 K and 623 K) and one higher (823 K). The key characteristics of the steamed FER28 samples are summarized in Table 5. Their XRD patterns and <sup>27</sup>Al NMR spectra are gathered in Figure S4. While steaming near the reaction

temperature does not result in any significant loss of crystallinity or structural changes, steaming at 823 K results in the loss of 20 % of tetrahedral Al. However, almost no octahedral Al is detected by NMR, suggesting that the extra-framework Al atoms are in a distorted environment preventing their detection.[38] Upon steaming, both external Brønsted acid site density and isobutanol dehydration rate constant decrease, indicating that these acid sites play an important role in the reaction. Finally, the absence of a significant impact of steaming at 523 and 623 K, *i.e.* close to the reaction temperature, on the total amount of acid sites highlights that overall the FER crystals are stable under our reaction conditions ( $T = 523$  K).

**Table 5.** Characteristics of FER28 steamed at 523, 623 and 823 K.

<b>Catalyst</b>	<b>FER28</b>	<b>523 K</b>	<b>623 K</b>	<b>823 K</b>
$B_{\text{tot}} - L_{\text{tot}}^a$ ( $\mu\text{mol g}^{-1}$ )	540 – 70	580 - 46	570 - 69	420 - 142
$B_{10\text{MR}} / B_{\text{tot}}^a$ (%)	53	48	56	51
$B_{\text{ext}} - L_{\text{ext}}^a$ ( $\mu\text{mol g}^{-1}$ )	17 – 11	13 - 12	8 - 11	7 - 5
$k$ ( $\text{mol h}^{-1} \text{g}_{\text{cat}}^{-1}$ )	1.50	1.36	0.95	0.61
$S_{\text{n-C4}}^b$ (%)	81.4	80.2	81.0	81.2

(<sup>a</sup> *in-situ* FT-IR, <sup>b</sup> at 50 % isobutanol conversion in a tubular PFR, reaction conditions:  $T = 523$  K,  $\text{WHSV} = 100 \text{ h}^{-1}$ ,  $P = 1$  bar,  $P_{\text{isobutanol}} = 45$  mbar,  $\text{TOS} = 4$  h)

#### *Isobutanol accessibility to the FER microporosity*

The isobutanol accessibility to the ferrierite microporosity can best be studied by monitoring isobutanol adsorption by *in-situ* IR spectroscopy at various temperatures. Figure 3a shows difference IR spectra (spectrum of the pristine zeolite subtracted from the spectra recorded after isobutanol adsorption) at room temperature after adsorption of 0.5 torr of isobutanol at a

temperature between 298 K - 573 K. Between 298 K to 373 K, isobutanol is only adsorbed on silanol groups as indicated by the negative band at  $3748\text{ cm}^{-1}$ . These silanol groups are mainly located on the external surface of the crystals. The IR band characteristic of Brønsted acid sites,  $3590\text{ cm}^{-1}$ , is unaffected suggesting that isobutanol does not enter the microporosity.[15]

However, at a temperature of 398 K, the intensity of this band starts decreasing. At the same time, three broad bands appear at  $2922$ ,  $2405$  and  $1672\text{ cm}^{-1}$ , characteristic of an ABC structure, indicating that above 398 K some internal Brønsted acid sites are involved in strong hydrogen bond. Such ABC structures result from Fermi resonances between the  $\nu(\text{OH})$  stretching mode of the bridged OH groups extending to low frequencies due to the formation of a strong hydrogen bonds (with isobutanol in the present case) and harmonic or combinations of the  $\delta(\text{OH})$  and  $\gamma(\text{OH})$  bending modes [39]. As isobutanol dehydration starts at 398 K (Figure 3b), the disappearance of Brønsted acid sites during *in-situ* IR experiments is due to their interactions with the dehydration products. An IR spectrum after water adsorption at room temperature on FER (Figure 3a, dotted line) confirms that the ABC structure is characteristic of water adsorption. Therefore, during the reaction, isobutanol does not significantly enter the microporosity; it reacts mostly on the external surface or at the pore mouths and only its dehydration products, water in particular, diffuse inside the zeolite pores.

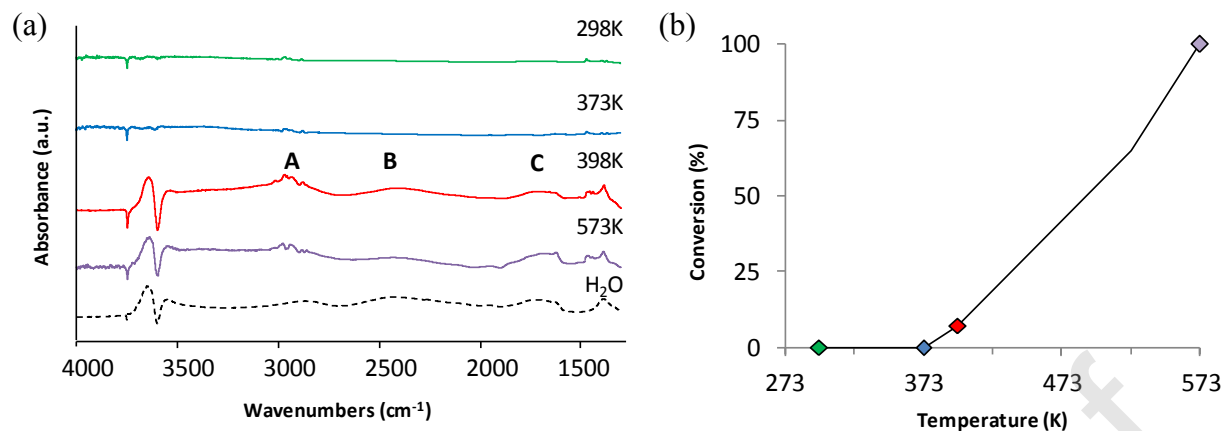


**Figure 3.** (a) Difference spectra after isobutanol adsorption and gas phase correction ( $P_{\text{sat}} = 0.5$  torr). (b) The effect of the reaction temperature on the conversion of isobutanol over ferrierite ( $P_{\text{C4}} = 0.045$  bar,  $\text{WHSV} = 103 \text{ h}^{-1}$ ).

#### *Impact of external surface acidity modifications*

As isobutanol does not penetrate the FER microporosity, external acid sites should be active in isobutanol dehydration and responsive to modifications of this acidity. To verify this, the external acid site density of FER28 was modified by two post-synthesis treatments to either decrease its overall external (Brønsted and Lewis) acidity or increase the Lewis/Brønsted acidity ratio. Decreasing the external acid site density was performed by chemical deposition of TEOS (tetra-ortho-ethylsilicate); the treatment was done once (1x TEOS) and repeated (2x TEOS). Increasing the Lewis/Brønsted acidity ratio was performed by chemical deposition of  $\text{Al}(\text{O}-i\text{Pr})_3$  (aluminum tri-isopropoxide).

The main features of the resulting FER zeolites are summarized in Table 6. They indicate that the external acidity can be significantly changed without impacting other properties of interest (micropore volume, total Brønsted and Lewis acidity). The slight changes in  $B_{\text{tot}}$  and  $L_{\text{tot}}$  could be due to the extra calcination steps undergone by the modified samples.

**Table 6.** Characteristics of external surface modified ferrierites.

Catalyst	FER28	1x TEOS	2x TEOS	1 x Al(O- iPr) <sub>3</sub>
B <sub>tot</sub> - L <sub>tot</sub> <sup>a</sup> (μmol g <sup>-1</sup> )	540 - 70	530 - 82	460 - 96	550 - 89
B <sub>10MR</sub> / B <sub>tot</sub> <sup>a</sup> (%)	53	51	50	49
B <sub>ext</sub> - L <sub>ext</sub> <sup>a</sup> (μmol g <sup>-1</sup> )	17 - 11	12 - 6	5 - 1	13 - 19
k (mol h <sup>-1</sup> g <sub>cat</sub> <sup>-1</sup> )	1.50	0.70	0.37	0.68
S <sub>n-C4</sub> <sup>b</sup> (%)	81.4	76.3	74.7	76.8

(<sup>a</sup> *in-situ* FT-IR, <sup>b</sup> at 50 % isobutanol conversion in a tubular PFR, reaction conditions: T = 523 K, WHSV = 100 h<sup>-1</sup>, P<sub>atm</sub> = 1 bar, P<sub>isobutanol</sub> = 45 mbar, TOS = 4 h)

These three post-synthesis treatments result in lower rate constants in isobutanol dehydration with respect to the parent FER28. The external Brønsted acid sites are, therefore, those active for isobutanol dehydration. In addition, the negative impact on the *n*-butene selectivity indicates a crucial role of the external surface acidity on the isomerization reaction.

#### *Role of the location of internal Brønsted acid sites*

As internal Brønsted acid sites in FER can be located either in 8 and 10 membered rings (MR), a selective poisoning could shed some light on their respective roles on *n*-butene selectivity during isobutanol conversion. A selective ion-exchange with sodium is commonly used to investigate that effect.[40,41]

Table 7 shows the main characteristics, catalytic properties of the parent zeolite (FER28) and its sodium exchanged derivatives.

**Table 7.** Characteristics of ferrierites with internal acidity modifications.

<b>Catalyst</b>	<b>FER28</b>	<b>30 % Na</b>	<b>60 % Na</b>	<b>86 % Na</b>	<b>96 % Na</b>
$B_{\text{tot}} - L_{\text{tot}}^a$ ( $\mu\text{mol g}^{-1}$ )	540 - 70	380 - 57	220 - 42	75 - 48	22 - 53
$B_{10\text{MR}} / B_{\text{tot}}^a$ (%)	53	75	98	88	100
$B_{\text{ext}} - L_{\text{ext}}^a$ ( $\mu\text{mol g}^{-1}$ )	17 - 11	15 - 11	16 - 14	18 - 11	17 - 14
$k$ ( $\text{mol h}^{-1} \text{g}_{\text{cat}}^{-1}$ )	1.50	1.48	1.24	1.12	1.00
$S_{\text{n-C4}}^b$ (%)	81.4	80.6	79	80.7	80.8

(<sup>a</sup> *in-situ* FT-IR, <sup>b</sup> at 50 % isobutanol conversion in a tubular PFR, reaction conditions: T = 523 K, WHSV = 100 h<sup>-1</sup>, P<sub>atm</sub> = 1 bar, P<sub>isobutanol</sub> = 45 mbar, TOS = 4 h)

A partial ion-exchange alters the ratio between the Brønsted acid sites located in the 8 and 10 MR. It confirms also a preferential location of sodium in the 8 MR channels, in agreement with Lercher *et al.*<sup>4</sup> This results in a decrease of the reaction rate without changing much *n*-butene selectivity, indicating that neither the density nor the location of internal Brønsted acid sites is critical in the isomerization step. However, as the water produced during isobutanol conversion increases sodium mobility, it may not remain in the 8 MR of FER under the reaction conditions, and no definitive conclusion can be drawn at this stage.[42]

#### *Role of the internal micropores*

The role of the micropore volume of Ferrierite can be studied by plugging it with carbonaceous deposits. Such a sample was prepared by deactivating a physical mixture of 80 % FER28 - 20 % silica in the conversion of isobutanol under industrial conditions. Table 8 indicates that while total and external Brønsted acid site density decrease, the micropore volume drops by 98 %, *i.e.* an almost complete plugging. The rate constant decreases, but to a smaller extent (75 %) while *n*-

butene selectivity is moderately affected (-10 %). Therefore, a possible role of carbonaceous species cannot be excluded.

**Table 8.** Selected properties of spent FER28.

Catalyst	FER28 Si	Spent
$B_{\text{tot}} - L_{\text{tot}}^{\text{a}}$ ( $\mu\text{mol g}^{-1}$ )	527 - 60	64 - 4
$B_{10\text{MR}} / B_{\text{tot}}^{\text{a}}$ (%)	51	9
$B_{\text{ext}} - L_{\text{ext}}^{\text{a}}$ ( $\mu\text{mol g}^{-1}$ )	15 -11	7 - 4
$C^{\text{b}}$ (%)	0.00	5.97
$V_{\text{micro}}$ ( $\text{cm}^3/\text{g}$ )	0.14	0.00004
$k$ ( $\text{mol h}^{-1} \text{g}_{\text{cat}}^{-1}$ )	1.40	0.34
$S_{n\text{-C4}}^{\text{c}}$ (%)	78.0	70.8

(<sup>a</sup> *in-situ* FT-IR, <sup>b</sup>TG, <sup>c</sup>at 50 % isobutanol conversion in a tubular PFR,

reaction conditions: T = 523 K, WHSV = 100 h<sup>-1</sup>, P<sub>atm</sub> = 1 bar, P<sub>isobutanol</sub> = 45 mbar, TOS = 4 h)

#### *Identification of surface species*

FER-based catalysts are known for their excellent isobutene selectivity in the *n*-butene skeletal isomerization reaction, *vide supra*. For *n*-butene to isobutene conversion, one hypothesis is that carbonaceous residues (“coke”) contain active sites.[12,37,43] Due to the similarities between the two reactions, assessing the contribution of such carbonaceous species to the activity could bring valuable insight into the reaction mechanisms. *Operando* IR spectroscopy is ideal for monitoring the formation of surface species at working conditions. Some difference IR spectra recorded during the first 4 hours of reaction – while deactivation with time on stream is continuous (Figure 1a) - are presented in Figure 4.

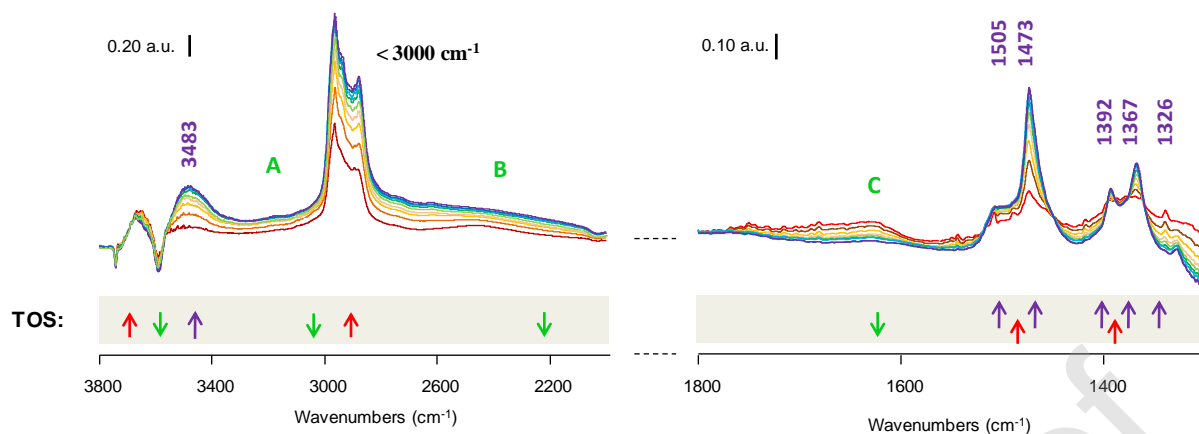


Figure 4. A selection ( $\Delta t = 30$  min) of difference IR spectra obtained during isobutanol conversion on FER28 with the gas phase isobutanol contributions (red), adsorption of water (green) and formation of deactivating species (purple). (reaction conditions:  $T = 525$  K,  $WHSV = 100$   $\text{h}^{-1}$ ,  $P_{\text{atm}} = 1$  bar,  $P_{\text{isobutanol}} = 45$  mbar, TOS = 4 h)

Chemometric analysis was used to extract valuable information from such a large number of spectra (*c.a.* 250). Principal component analysis (PCA) and multivariate curve resolution analysis (MCR-ALS) have been used for this purpose. PCA indicates that the first component captures a major part of the variance of the spectra (99.53 %), which is typical in the case of closely related spectra [32]. The following components captured 0.30%, 0.12% and 0.03% of the variance, suggesting that the number of components  $n$  required to describe adequately the experimental data lies between 1 and 4. This number was chosen on the basis of the residuals  $E$  between the matrix  $X_{1700-1400}$  of experimental spectra and the matrix  $\hat{X}_{1700-1400}$  of their estimates by MCR-ALS. As shown in Figure S5 of the supplementary information section, the use of two components vs. one yields a significant improvement of the modeling of the spectra, while the addition of a third or fourth component does not improve much the model. In particular the sum of residuals was of the same order of magnitude: (50 and 100 for two and three components vs.  $10^3$  for a single component). Further, as shown in Figure S6, the evolution of the

residuals with time on stream was similar for 2 and 3 components with a maximum located at the beginning of the reaction (0-5 minutes time on stream). This suggests that the use of two components is optimal for the modeling of these experimental spectra by MCR-ALS.

The MCR-ALS modeling of the spectra in the 1700-1400  $\text{cm}^{-1}$  range, yielded the matrix of concentration profiles  $C$  (Figure 5c) which in turn, was used to compute the matrix of pure spectral profiles  $S^T$  over the whole spectral range (Figure 5d). The matrix of reconstructed spectra  $\hat{X}$  was finally computed using:  $\hat{X} = C S^T$ . Figure 5b compares the experimental and reconstructed spectra from the concentration and spectral profiles shown in Figure 5c and d. Such a comparison allows a visual inspection of the model quality. Here, the residuals are significantly higher than the experimental noise and are mostly observed for the three spectra in the  $\nu\text{OH}$ ,  $\nu\text{CH}$  and  $\nu\text{CC}$  range, which could be accounted by the non-steady flow conditions that prevail at short reaction time ( $< 5$  mins). While this transitional regime would certainly be worth being studied, the time resolution of the spectra acquisition ( $> 1$  min) and, above all, the products analysis ( $> 5$  min) did not allow us to carry out such an analysis. On the other hand, an excellent agreement between experimental and reconstructed spectra was found above 10 minutes of reaction and no significant improvement was obtained when using a third component to describe the experimental spectra.

Examination of the first pure spectral profile of  $S^T$  shows two negative bands (3746 and 3590  $\text{cm}^{-1}$ ) indicating the consumption of terminal silanols and Brønsted acid sites, respectively. Additionally, an ABC structure is visible at 2935, 2447, and 1631  $\text{cm}^{-1}$ , indicating that Brønsted acid sites are hydrogen-bonded with water.[39] The positive bands at 3672, 3029 - 2806, 1473

and  $1392\text{ cm}^{-1}$  belong to isobutanol. The first component represents therefore the interaction of isobutanol and water with the zeolite. As water is a primary product of the reaction, we cannot exclude that other products (butenes) appear alongside water and contribute also to this component. However, as shown in Figure 6 below, isobutene does not enter the FER microporosity. Moreover, when iso- and *n*-butenes are fed to the catalyst at the same temperature and pressure, their peak intensities are substantially lower than those observed with isobutanol (Figure 6), suggesting that these butenes promptly desorb after their formation and do not contribute significantly to the difference spectral profiles.

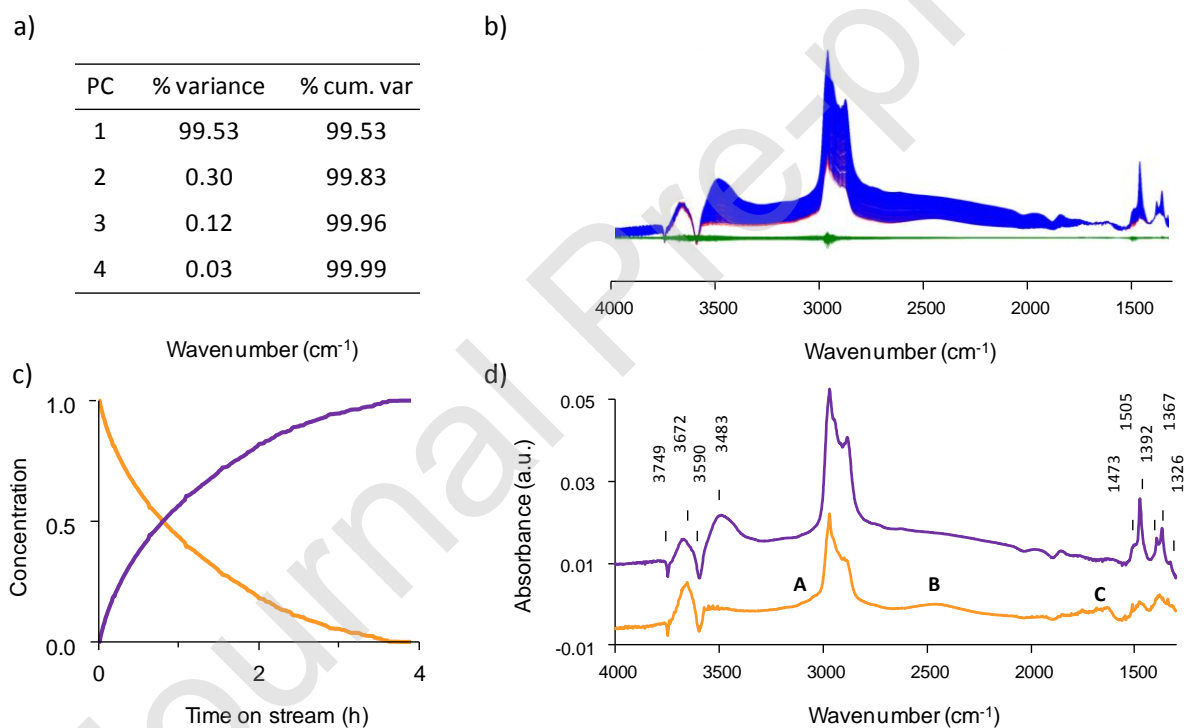


**Figure 5.** PCA and MCR-ALS on the isobutanol conversion over FER28 ( $T = 525\text{ K}$ ,  $\text{WHSV} = 100\text{ h}^{-1}$ ,  $P_{\text{atm}} = 1\text{ bar}$ ,  $P_{\text{isobutanol}} = 45\text{ mbar}$ ,  $\text{TOS} = 4\text{ h}$ ) a) Overview of the percentage of variance explained per principal component (PC) b) Reconstruction of the experimental spectra from the pure species obtained by MCR-ALS. Red: experimental spectra X, Blue: reconstructed spectra

$\hat{X}$ , Green: residuals E c) MCR-ALS concentration profile and d) the pure difference spectral profiles reconstructed using MCR-ALS (first profile: orange, second profile: purple)

The second component shows the silanol and Brønsted acid site consumption at 3749 and 3590  $\text{cm}^{-1}$ , and the formation of new bands at 3483, 1505, 1473, 1392, 1367 and 1326  $\text{cm}^{-1}$ . The 3483  $\text{cm}^{-1}$  band is characteristic of H-bonded bridged hydroxyl groups and can be formed due to the interaction of Brønsted acid sites with a single or a set of species with absorptions at 1505, 1473, 1392, 1367 and 1326  $\text{cm}^{-1}$ . These bands belong either to a single adsorbed species or to a set of adsorbed species whose relative concentrations remain constant during the reaction. The appearance of the band at 3483  $\text{cm}^{-1}$ , characteristic of H-bonded bridged OH groups and the simultaneous disappearance of the ABC structure suggests that the interaction between the Brønsted acid sites and water is systematically replaced with the new set of species. This is confirmed by the evolution of the MCR-ALS concentration profiles of pure species (Figure 5c).

Figure 6 compares the IR spectrum obtained under *operando* conditions after four hours of isobutanol reaction with the one after a 20 minutes nitrogen purge. It clearly indicates that most of these species are strongly adsorbed on the catalyst surface.

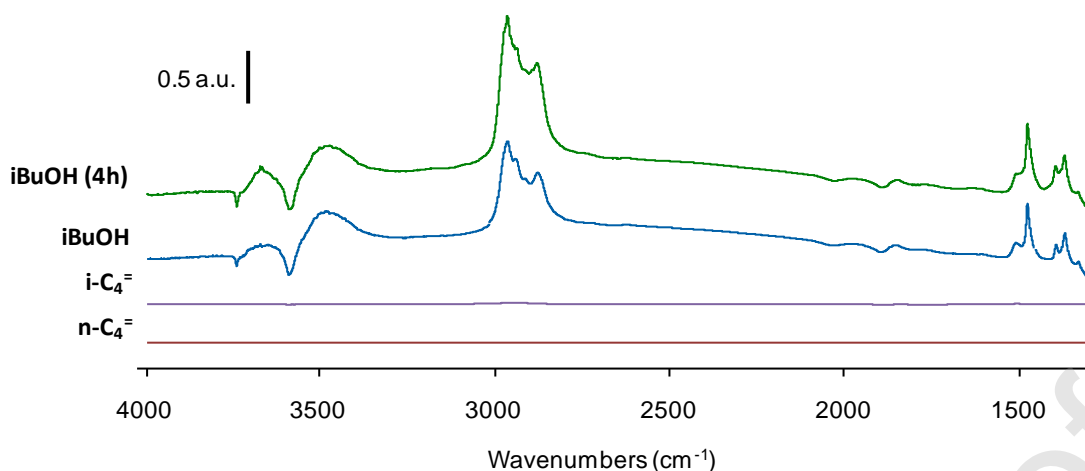


**Figure 6.** Difference IR spectra during isobutanol conversion on FER28, (green) 4 hours of reaction, (blue) Nitrogen purge for 20 minutes ( $25 \text{ cc. min}^{-1}$ ) (FER28,  $T = 525 \text{ K}$ ,  $\text{WHSV} = 100 \text{ h}^{-1}$ ,  $P = 1 \text{ bar}$ ,  $P_{\text{isobutanol}} = 45 \text{ mbar}$ ,  $\text{TOS} = 4 \text{ h}$ ), (purple) Nitrogen purged ( $25 \text{ cc. min}^{-1}$ ) difference spectra after reaction with isobutene, (red) Nitrogen purged ( $25 \text{ cc. min}^{-1}$ ) difference spectra after reaction with *n*-butene. Both are corrected to 0.045 bar of  $\text{C}_4$  pressure (FER28,  $T = 525 \text{ K}$ ,  $\text{WHSV} = 0.007 \text{ h}^{-1}$ ,  $P = 1 \text{ bar}$ ,  $P_{\text{C}_4} = 1 \text{ bar}$ ,  $\text{TOS} = 4 \text{ h}$ )

At the timescale and under the reaction conditions of the *operando* IR experiments (one spectrum recorded each 42 s over 4 hours of reaction), no significant change of the nature of this/these species is evidenced. The absence of bands in the  $3000 - 3100 \text{ cm}^{-1}$  range allows to conclude that the corresponding species are most probably not aromatic, in agreement with Paze *et al.* who studied 1-butene isomerization at similar reaction temperatures.[44] The extent of the  $\Delta\nu(\text{OH})$  shift between the frequency of the free Brønsted acid sites and the band at  $3483 \text{ cm}^{-1}$  provides additional information on the nature of these interacting species. This shift ( $118 \text{ cm}^{-1}$ ) is similar to that observed upon adsorption of *n*-hexane while the shift observed upon adsorption of other classes of compounds are much larger (water :  $712 \text{ cm}^{-1}$  and ABC structure, alkane :  $118 \text{ cm}^{-1}$ , alkene :  $\sim 700 \text{ cm}^{-1}$ , alkyne :  $220 \text{ cm}^{-1}$ ).[45,46] Quantification of the frequency shift

resulting from the interaction with an aromatic carbon ring was not successful since the smallest aromatic compound, benzene, cannot access the microporous volume. The absence of a  $\nu(\text{OH})$  band characteristic of alkene adsorption ( $\Delta\nu(\text{OH}) \sim 700 \text{ cm}^{-1}$ ) under such reaction conditions, might be explained by i) the small number of light alkenes adsorbed, ii) a proton transfer to the alkene moieties of strongly adsorbed species.

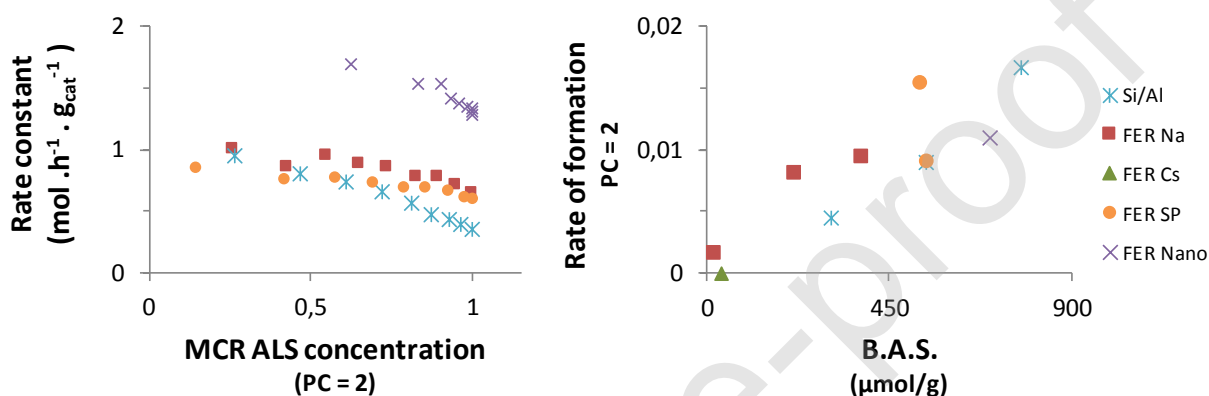


**Figure 7.** (a) Evolution of the rate constant versus the MCR-ALS concentration of the second pure species (PC = 2), (b) Relationship between the rate of formation of the second pure species and total Brønsted acidity, (reaction conditions:  $T = 525 \text{ K}$ ,  $\text{WHSV} = 100 \text{ h}^{-1}$ ,  $P_{\text{atm}} = 1 \text{ bar}$ ,  $P_{\text{isobutanol}} = 45 \text{ mbar}$ ,  $\text{TOS} = 4 \text{ h}$ )

In order to determine if such species have a direct impact on catalytic activity, the reaction rates and the product yields have been compared to the evolution of the MCR-ALS concentration profiles of these species. As shown in figure 7a, a weak and negative correlation was found between the reaction rate of isobutanol and the MCR-ALS concentration of the second pure species. This suggests that most of these species are not directly involved in the deactivation. Moreover, no correlation was observed between the MCR-ALS concentration of these species and the product yields or selectivities.

In order to determine the nature of the sites involved in the formation of these species, their initial rate of formation – as determined by the variation of the MCR-ALS concentration over the first 30 minutes of reaction was compared to the concentrations of acidic sites.

Figure 7 shows that a significant linear correlation holds between the rate of formation of the second pure species and the total Brønsted acid site concentration of the samples. This is a strong indication that these carbonaceous species are produced by reactions involving the products of isobutanol dehydration on Brønsted acid sites.

#### *Impact of morphology*

As the external Brønsted acidity of FER appears to play an important role in the isomerization reaction, the effect of particle size and shape (needle and plate-like shape) on catalytic performances should shed further insight in mechanisms.[19,20] While decreasing crystal size increases the specific external surface area, modifying crystal morphology can affect the ratio between the different types of pore mouths, 8 vs. 10 MR. Two FER zeolites with a nanoplate and a nanoneedle morphology were prepared and tested in isobutanol conversion; their relevant properties are reminded in Table 9. As the nanosized samples have a high aluminum content, they are best compared with FER9.

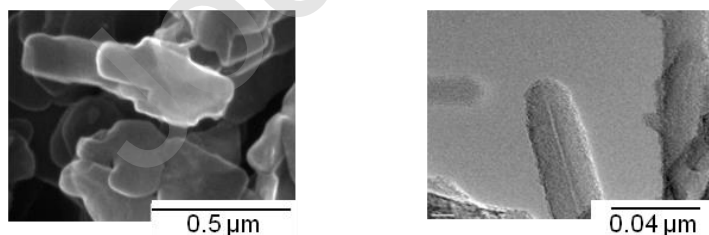


**Figure 8.** SEM picture of FER nanoplate (left), TEM picture of FER nanoneedle (right)

Table 9 shows that *n*-butenes selectivity changes for both nanocrystals. Despite the increased external surface (more pore mouths), there is no correlation with the *n*-butenes selectivity. Moreover, this selectivity does not follow the same trend as the external Brønsted acidity. This indicates that the superior *n*-butenes selectivity of Ferrierite cannot just be explained by the number of external Brønsted acid sites.

Journal Pre-proof

**Table 9.** Characteristics of nanosized Ferrierites.

Catalyst	FER 9	Nanoneedle	Nanoplate
$S_{\text{ext}}$ ( $\text{m}^2 \text{g}^{-1}$ )	25	240	42
$B_{\text{tot}} - L_{\text{tot}}$ <sup>a</sup> ( $\mu\text{mol g}^{-1}$ )	770 – 795	688 - 275	697 - 937
$B_{10\text{MR}} / B_{\text{tot}}$ <sup>a</sup> (%)	16	5	28
$B_{\text{ext}} - L_{\text{ext}}$ <sup>a</sup> ( $\mu\text{mol g}^{-1}$ )	26 – 6	36 - 85	17 - 13
$k$ ( $\text{mol h}^{-1} \text{g}_{\text{cat}}^{-1}$ )	3.13	5.21	3.99
$S_{\text{n-C4}}$ <sup>b</sup> (%)	80.4	75.4	84.1

<sup>a</sup> *in-situ* FT-IR, <sup>b</sup> at 50 % isobutanol conversion in a tubular PFR, reaction conditions: T = 523 K, WHSV = 100 h<sup>-1</sup>, P = 1 bar, P<sub>isobutanol</sub> = 45 mbar, TOS = 4 h)

#### *Study of butene isomerization*

Next, the isomerization reactions involved in the one-step conversion were studied to gain a better comprehension of this multistep reaction. The conversions of iso- and *n*-butenes were compared on the FER28 catalyst under identical conditions. As shown in **Figure 9**, two possible reaction mechanisms for the one-step dehydration of isobutanol over Ferrierite can be considered, namely a *direct* (red) or *indirect* (blue) formation of *n*-butenes.

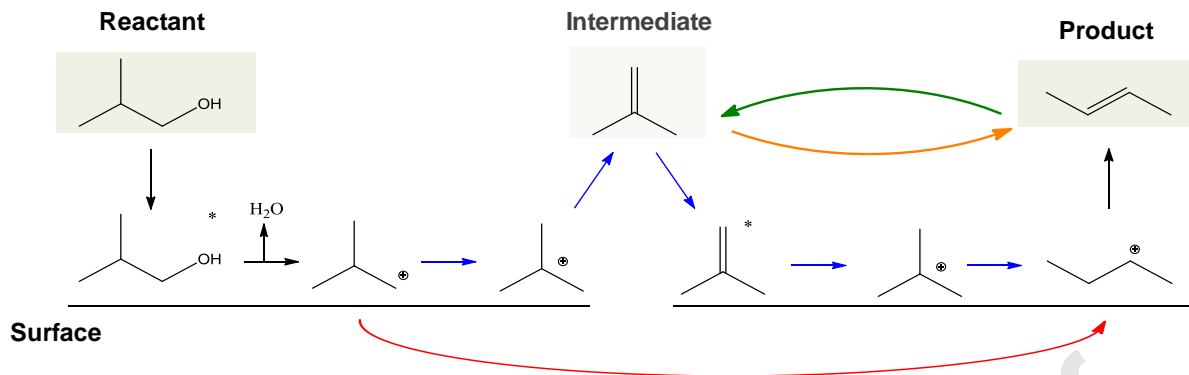


**Figure 9.** Reaction scheme for the one-step conversion of isobutanol into butenes. Direct (Red) and indirect (Blue) formation of *n*-butenes from isobutanol. Isomerization of *n*-butenes to isobutene (Green) and isobutene to *n*-butenes (Orange)

Since a stable isobutene intermediate is formed in the indirect pathway, a rake-type mechanism could be considered (blue arrows, **Figure 9**). The reaction starts with isobutanol dehydration and the formation of a primary carbocation. It must then undergo a 1,2 - rearrangement to form a more stable ion. While both a proton and methyl shifts are valid options, the proton shift is expected to occur more rapidly [9]. However, this will form a more stable tertiary carbocation yielding isobutene after deprotonation. To obtain *n*-butenes, a consecutive isomerization step is required. On the other hand, in the direct mechanism (red arrow), the slower methyl shift does not require any further isomerization. The zeolite external surface can provide some additional stabilization of the carbocation favoring the methyl shift and the direct formation of *n*-butenes. The latter can then isomerize into isobutene as a side reaction (green arrow); it is thus worthwhile to compare the kinetics of isobutanol conversion with that of butene isomerization.

The rate constants of each reactions were measured on the reference ferrierite (FER28) sample at the same temperature used for isobutanol conversion and presented in Table 10. The rate

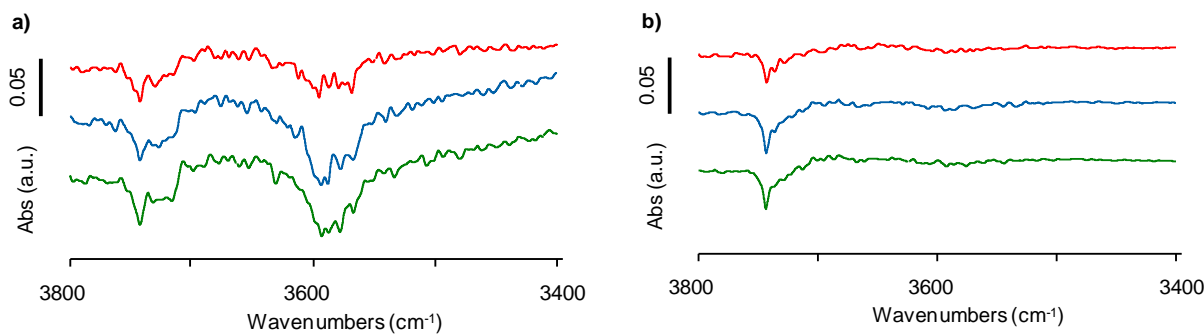
constants for isomerization of branched and linear butenes are about two orders of magnitude lower than for the transformation of isobutanol to *n*-butenes. This indicates that these steps do not participate in the transformation of isobutanol to *n*-butene and a rake-type mechanism can be discarded. Hence, isomerization and dehydration must either occur simultaneously on a single site of the surface or occur sequentially. In the latter case, isomerization should occur *before* formation of isobutene from the *iso*- and *tert*-butyl cations (or their corresponding alkoxides) formed after the dehydration step. This implies that the alkoxide intermediate is stabilized on the surface to prevent its desorption before its isomerization, or that dehydration and isomerization sites – if distinct - are in close proximity.

**Table 10.** Comparison of pseudo-first order kinetic rate constants at 525 K

<b>Reaction</b>	Isobutanol to all products	Isobutanol to <i>n</i> -butene	Isobutene to <i>n</i> -butene	<i>n</i> -butene to isobutene
WHSV (h <sup>-1</sup> )	100	100	0.01	0.01
P (bar)	0.05	0.05	1.00	1.00
rate constant (mol.h <sup>-1</sup> . g <sub>cat</sub> <sup>-1</sup> .bar <sup>-1</sup> )	21.28	15.55	0.01	0.02

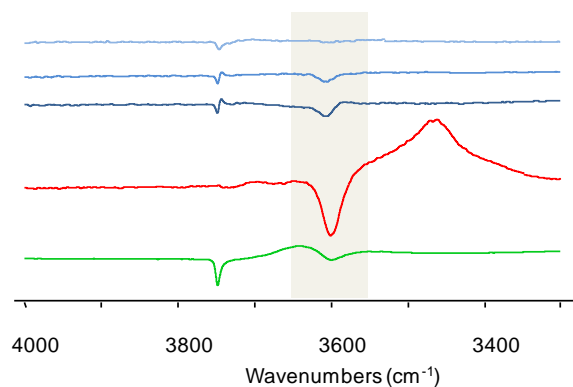
(*operando* reactor, FER28, P<sub>atm</sub> = 1 bar, TOS = 4 h)

Figure 10 shows the difference spectra obtained in the *operando* IR cell during the transformations of trans-2-butene and isobutene over FER. For the isomerization of *n*-butenes, the spectra display two negative bands at 3742 cm<sup>-1</sup> and 3590 cm<sup>-1</sup>, evidence of the progressive and irreversible consumption of silanol groups and Brønsted acid sites.



**Figure 10.** Difference IR spectra (saturation - reference) of FER28 during the skeletal isomerization of a) trans-2-butene and b) isobutene after 10 minutes (red), 4 hours (blue) and a 20-minute (green) nitrogen purge. (*operando* reactor, FER28,  $T = 525$  K,  $WHSV = 0.007$  h<sup>-1</sup>,  $P_{tot} = 1$  bar,  $P_{C4} = 1$  bar, TOS = 4 h)

The spectra recorded during isobutene isomerization show the absence of a negative band at  $3590$  cm<sup>-1</sup>, clearly visible during *n*-butene isomerization. The absence of this band suggests that isobutene does not enter the ferrierite microporosity under our reaction conditions. This hypothesis can be confirmed by the spectra obtained after isobutene adsorption at various temperatures (Figure 11). In all cases, a negligible amount of isobutene reacts ( $\approx 1$  %). For comparative purpose, difference spectra obtained after consumption of the external acid sites by 2,6-dimethylpyridine adsorption[47] and after consumption of the 10 MR Brønsted acid sites by *n*-hexane are added.<sup>22</sup>



**Figure 11.** Difference *in-situ* IR spectra after adsorption on FER of 0.5 torr of isobutene (blue top: 298 K, middle: 473 K, bottom: 573 K), *n*-hexane at 298 K (red) and 2,6-dimethylpyridine at 298 K (green)

Figure 11 indicates that the quantity of Brønsted acid sites consumed by isobutene and 2-6 dimethyl pyridine (probing only the external Brønsted acidity of medium pore zeolites[47]) are very close. Isobutene therefore does not access significantly the Ferrierite microporosity and if formed in the microporosity, it would diffuse very slowly to the external surface. As isobutanol cannot either access the microporosity, this further indicates the key role of the external acidity for the one-step conversion of isobutanol into linear butenes.

#### *Structure-activity relationship in isobutanol conversion to n-butenes*

The above results identify unambiguously the external Brønsted acid sites as active sites for the dehydration of isobutanol as this reactant cannot access the Ferrierite microporosity and their subsequent involvement in the consecutive isomerization step. **Error! Reference source not found.**a shows that the initial dehydration rate constants of the various FER investigated in this work are strongly correlated to their external Brønsted acid site concentration. The latter encompass the Brønsted acid sites which can be probed by 2,6-lutidine i.e. those located on the external surface and at the pore mouth.

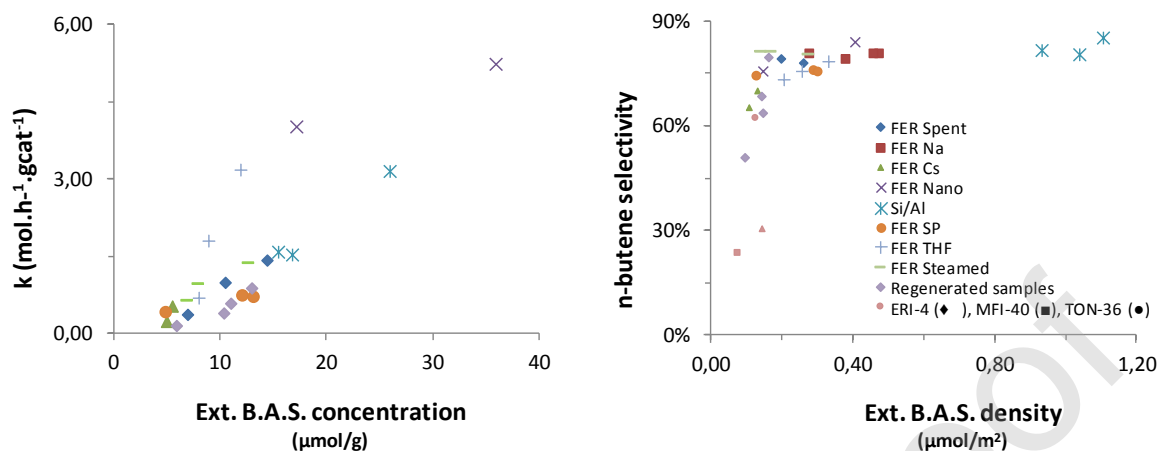


**Figure 12** (a) Effect of the external Brønsted acid site concentration on the initial dehydration rate constant (b) Effect external Brønsted acid site density on *n*-butene selectivity (reaction conditions: classic reactor,  $T = 523$  K,  $\text{WHSV} = 100$   $\text{h}^{-1}$ ,  $P_{\text{atm}} = 1$  bar,  $P_{\text{isobutanol}} = 45$  mbar,  $\text{TOS} = 4$  h). The method of preparation and characteristics of FER THF, FER Cs and regenerated samples are summarized in the supporting information.

A direct relation between the quantity of external Brønsted acid sites concentration and the *n*-butene selectivity however, is not found. The possible mechanisms discussed in the previous section suggest that the proximity between external Brønsted acid sites can play a key role in explaining the high *n*-butene selectivity. **Error! Reference source not found.** b highlights the relationship between the external Brønsted acid sites density and *n*-butene selectivity for all the FER-type zeolites investigated in this work. There is a steep variation of *n*-butene selectivity (from  $\sim 20$  % to  $\sim 80$  %) for the zeolites with the lowest external Brønsted acid site density ( $< 0.20$   $\mu\text{mol m}^{-2}$ ), while beyond a threshold value of about  $0.20$   $\mu\text{mol m}^{-2}$ , the *n*-butene selectivity reaches a plateau ( $\sim 80$  %) with no further increase with the Brønsted acid sites density.

Remarkably, the three zeolites presenting other pore topologies, namely ERI (8 MR), MFI (10 MR) and TON (10 MR) follow the same general trend observed for the FER zeolites. This suggests that the excellent selectivity of Ferrierite is a result of its high external Brønsted acid sites density. Close proximity between Brønsted acid sites could prevent fast desorption of adsorbed *iso*- and *tert*-butyl cations (or their corresponding alkoxides) and therefore the formation of isobutene. Another possibility is that a high external surface density of Brønsted acid sites could statistically favor the formation of vicinal, paired Brønsted acid sites acting as single active sites.

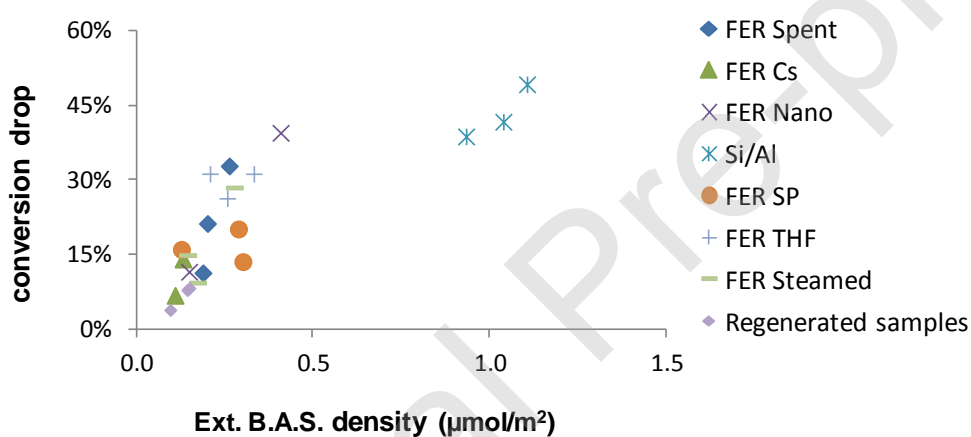


**Figure 13.** Effect of external Brønsted acid density on the conversion drop. (reaction conditions: tubular PFR,  $T = 525 \text{ K}$ ,  $\text{WHSV} = 100 \text{ h}^{-1}$ ,  $P_{\text{atm}} = 1 \text{ bar}$ ,  $P_{\text{isobutanol}} = 45 \text{ mbar}$ ,  $\text{TOS} = 4 \text{ h}$ )

Despite an improved selectivity, however, the increase in external Brønsted acid site density has a negative impact on the catalyst stability. This is illustrated in Figure which correlates the conversion drop after 4 hours time-on-stream with the external Brønsted acid sites density. This correlation suggests that the deactivating species are formed by secondary reactions involving neighboring external Brønsted acid sites. A higher density of external Brønsted acid sites, *i.e.* a smaller distance between these sites, results in a more significant drop in conversion. This

suggests that optimizing the density of external Brønsted acid sites of the zeolite is critical to combine a high conversion with maximum selectivity and a moderate deactivation in the conversion of isobutanol to isobutene.

## Conclusions

In the newly developed ATOL-C4<sup>TM</sup> process, bio-sourced linear butenes are generated from isobutanol with high selectivity after a one-step dehydration and skeletal isomerization. A more fundamental understanding of the separate reactions at play (dehydration and isomerization) was required to design better performing catalysts. Due to the similarities with the isomerization of *n*-butenes to isobutene, the possible involvement of the formed carbon pool could not be excluded. By combining state-of-the-art *operando* spectroscopy with a chemometric analysis (PCA and MCR-ALS), time-resolved information on the carbonaceous species formation was extracted out of the complex data mixture. Since these data are not correlated with the evolving *n*-butene selectivity, this strongly suggests that carbonaceous species do not participate in the isomerization step as for pseudo-monomolecular mechanism proposed for *n*-butene isomerization. Next, the reactions involved in the one-step isobutanol conversion were studied to gain a better comprehension of this multistep reaction. By fine-tuning acidity (Lewis, Bronsted, external, 10 or 8MR channel...), morphological and textural properties of FER samples, a library of modified Ferrierites was built in order to evaluate the main factors influencing the catalytic performances. The impact of the modifications was carefully quantified using a systematic *in-situ* IR analysis with specific probe molecules. The combination with catalytic testing allowed establishing that neither isobutanol nor isobutene enter the ferrierite internal structure. However, a linear relationship was found between the Brønsted acid sites located on (or close to) the

external surface and the dehydration rate constant. We suggest those acid sites are the isobutanol dehydration active sites. Afterward, a comparison of pseudo-first-order rate constant for isobutene isomerization and isobutanol to *n*-butene transformation allowed to exclude isobutene as an intermediate (which would lead to a much slower rate) and the initially imagined rake-type mechanism. Therefore, it was proposed that proximity between the dehydration and isomerization active site is required to avoid desorption of intermediate carbocation prior to isomerization occurring. Finally, proximity between external Brønsted acid sites was found to have a major impact on the selectivity toward *n*-butene and it can be concluded that a threshold surface density of external Brønsted acid sites is required to obtain a high selectivity in *n*-butene selectivity. The existence of this threshold explains the exceptional *n*-butene selectivity of FER-type zeolites in comparison with other 10 MR zeolites such as MFI- or TON-type. In conclusion, this study allowed identifying the sites responsible for both the dehydration of isobutanol and the consecutive isomerization step and proposing a mechanism for this one-step reaction. The information gathered in this study offers insights to optimize the next generation of industrial catalysts for the dehydration of isobutanol to linear butenes.

### **Declaration of interests**

The authors declare that they have no known competing financial interests or personal relationships that could have appeared to influence the work reported in this paper.

Credit Author statement :

**Stijn van Daele** : Conceptualization, Investigation , Software, Validation, Formal analysis, Data Curation, Writing - Original Draft, Writing - Review & Editing.

**Delphine Minoux** : Conceptualization, Writing - Review & Editing, Supervision

**Nikolai Nesterenko** : Conceptualization, Writing - Review & Editing, Supervision, Project administration, Funding acquisition

**Sylvie Maury**: Conceptualization, Writing - Review & Editing,

**Vincent Coupard**: Conceptualization, Writing - Review & Editing,

**Valentin Valtchev**: Conceptualization, Writing - Original Draft, Writing - Review & Editing,

**Arnaud Travert**: Conceptualization, Investigation, Software, Validation, Formal analysis, Data Curation, Writing - Original Draft, Writing - Review & Editing

**Jean-Pierre Gilson**: Conceptualization, Writing - Original Draft, Writing - Review & Editing, Project administration, Funding acquisition

### Acknowledgments

This work was made possible by a CIFRE PhD grant (S. van Daele) from Total Research and Technology Feluy (TRTF) and Agence Nationale de la Recherche Technologique (France, 2015/0177).

**References**

- [1] P.C.A. Bruijninx, B.M. Weckhuysen, Shale Gas Revolution : An Opportunity for the Production of Biobased Chemicals ?, *Angew. Chemie - Int. Ed.* 52 (2013) 11980–11987. <https://doi.org/10.1002/anie.201305058>.
- [2] I. Amghizar, L.A. Vandewalle, K.M. Van Geem, G.B. Marin, New Trends in Olefin Production, *Engineering*. 3 (2017) 171–178. <https://doi.org/10.1016/J.ENG.2017.02.006>.
- [3] C.T. Chen, J.C. Liao, Frontiers in microbial 1-butanol and isobutanol production, *FEMS Microbiol. Lett.* 363 (2016) 1–13. <https://doi.org/10.1093/femsle/fnw020>.
- [4] H. Knözinger, H. Bühl, E. Ress, The dehydration of alcohols over alumina: VII. The dependence of reaction direction on the substrate structure, *J. Catal.* 12 (1968) 121–128. [https://doi.org/10.1016/0021-9517\(68\)90084-5](https://doi.org/10.1016/0021-9517(68)90084-5).
- [5] H. Knözinger, R. Köhne, The Dehydration of Alcohols over Alumina : I. The Reaction Scheme, *J. Catal.* 5 (1966) 264–270. [https://doi.org/10.1016/s0021-9517\(66\)80007-6](https://doi.org/10.1016/s0021-9517(66)80007-6).
- [6] H. Knözinger, H. Bühl, K. Kochloefl, The dehydration of alcohols on alumina: XIV. Reactivity and mechanism, *J. Catal.* 24 (1972) 57–68. [https://doi.org/http://dx.doi.org/10.1016/0021-9517\(72\)90007-3](https://doi.org/http://dx.doi.org/10.1016/0021-9517(72)90007-3).
- [7] J.D. Taylor, M.M. Jenni, M.W. Peters, Dehydration of Fermented Isobutanol for the Production of Renewable Chemicals and Fuels, *Top. Catal.* 53 (2010) 1224–1230. <https://doi.org/10.1007/s11244-010-9567-8>.
- [8] V. Macho, M. Králik, E. Jurecekova, J. Hudec, L. Jurecek, Dehydration of C4 alkanols conjugated with a positional and skeletal isomerisation of the formed C4 alkenes, *Appl.*

- Catal. A Gen. 214 (2001) 251–257. [https://doi.org/10.1016/S0926-860X\(01\)00497-5](https://doi.org/10.1016/S0926-860X(01)00497-5).
- [9] N.S. Kotsarenko and L.V. Malysheva, *Kinet. i Katal.* (1983) 877–882.
- [10] D. Zhang, S. a I. Barri, D. Chadwick, N-Butanol to iso-butene in one-step over zeolite catalysts, *Appl. Catal. A Gen.* 403 (2011) 1–11.  
<https://doi.org/10.1016/j.apcata.2011.05.037>.
- [11] C. Adams, D. Minoux, K. Nesterenko, S. Van Donk, J.-P. Dath, Simultaneous dehydration and skeletal isomerisation of isobutanol on acid catalysts, WO 2011/113834 A1, 2011.
- [12] M. Guisnet, P. Andy, Y. Boucheffa, N.S. Gnep, C. Travers, E. Benazzi, Selective isomerization of n-butenes into isobutene over aged H-ferrierite catalyst: nature of the active species, *Catal. Letters.* 50 (1998) 159–164.  
<https://doi.org/10.1023/A:1019052026632>.
- [13] C.-L. O’Young, R.J. Pellet, D.G. Casey, J.R. Ugolini, R.A. Sawicki, Skeletal isomerization of 1-butene on 10-member ring zeolite catalysts, *J. Catal.* 151 (1995) 467–469. <https://doi.org/10.1006/jcat.1995.1051>.
- [14] L. Domokos, L. Lefferts, K. Seshan, J. Lercher, The importance of acid site locations for n-butene skeletal isomerization on ferrierite, *J. Mol. Catal. A Chem.* 162 (2000) 147–157.  
[https://doi.org/10.1016/S1381-1169\(00\)00286-7](https://doi.org/10.1016/S1381-1169(00)00286-7).
- [15] S. Van Donk, E. Bus, A. Broersma, J.H. Bitter, K.P. De Jong, Probing the Accessible Sites for n-Butene Skeletal Isomerization over Aged and Selective H-Ferrierite with d3-Acetonitrile, *J. Catal.* 212 (2002) 86–93. <https://doi.org/10.1006/jcat.2002.3767>.
- [16] P. Meriaudeau, R. Bacaud, L. Ngoc Hung, A.T. Vu, Isomerization of butene in isobutene

- on ferrierite catalyst: A mono- or a bimolecular process?, *J. Mol. Catal. A Chem.* 169 (1996) 2–4. [https://doi.org/10.1016/1381-1169\(96\)00156-2](https://doi.org/10.1016/1381-1169(96)00156-2).
- [17] Z. Buniazet, A. Cabiac, S. Maury, D. Bianchi, S. Loridant, Unexpected selectivity of FER for the conversion of isobutanol to linear butenes and water effects, *Appl. Catal. B, Environ.* 243 (2019) 594–603. <https://doi.org/10.1016/j.apcatb.2018.11.007>.
- [18] D. Minoux, N. Nesterenko, S. Van donk, J.-P. Dath, C. Adam, Process to make olefins from isobutanol, EP 2 601 158 B1, 2012.
- [19] Y. Lee, M.B. Park, P.S. Kim, A. Vicente, C. Fernandez, I.S. Nam, S.B. Hong, Synthesis and catalytic behavior of ferrierite zeolite nanoneedles, *ACS Catal.* 3 (2013) 617–621. <https://doi.org/10.1021/cs400025s>.
- [20] E. Catizzone, S. Van Daele, M. Bianco, A. Di Michele, A. Aloise, M. Migliori, V. Valtchev, G. Giordano, Catalytic application of ferrierite nanocrystals in vapour-phase dehydration of methanol to dimethyl ether, *Appl. Catal. B, Environ.* 243 (2019) 273–282. <https://doi.org/10.1016/j.apcatb.2018.10.060>.
- [21] A.K. Jamil, O. Muraza, Facile control of nanosized ZSM-22 crystals using dynamic crystallization technique, *Microporous Mesoporous Mater.* 227 (2016) 16–22. <https://doi.org/10.1016/j.micromeso.2016.02.005>.
- [22] P. Losch, M. Boltz, C. Bernardon, B. Louis, A. Palčić, V. Valtchev, Impact of external surface passivation of nano-ZSM-5 zeolites in the methanol-to-olefins reaction, *Appl. Catal. A Gen.* 509 (2016) 30–37. <https://doi.org/10.1016/j.apcata.2015.09.037>.
- [23] B. Wichterlová, Z. Tvarůžková, Z. Sobalík, P. Sarv, Determination and properties of acid

- sites in H-ferrierite: A comparison of ferrierite and MFI structures, *Microporous Mesoporous Mater.* 24 (1998) 223–233. [https://doi.org/10.1016/S1387-1811\(98\)00167-X](https://doi.org/10.1016/S1387-1811(98)00167-X).
- [24] T. Montanari, M. Bevilacqua, G. Busca, Use of nitriles as probe molecules for the accessibility of the active sites and the detection of complex interactions in zeolites through IR spectroscopy, *Appl. Catal. A Gen.* 307 (2006) 21–29. <https://doi.org/10.1016/j.apcata.2006.03.003>.
- [25] K. Sadowska, K. Góra-Marek, J. Datka, Accessibility of acid sites in hierarchical zeolites: Quantitative IR studies of pivalonitrile adsorption, *J. Phys. Chem. C.* 117 (2013) 9237–9244. <https://doi.org/10.1021/jp400400t>.
- [26] F. Eder, J. Lercher, On the role of the pore size and tortuosity for sorption of alkanes in molecular sieves, *J. Phys. Chem. B.* 5647 (1997) 1273–1278. <https://doi.org/10.1021/jp961816i>.
- [27] P. Magnoux, P. Cartraud, S. Mignard, M. Guisnet, Coking, aging, and regeneration of zeolites. II. Deactivation of HY zeolite during n-heptane cracking, *J. Catal.* 106 (1987) 235–241. [https://doi.org/10.1016/0021-9517\(87\)90227-2](https://doi.org/10.1016/0021-9517(87)90227-2).
- [28] H. Li, M. Rivallan, F. Thibault-Starzyk, A. Travert, F.C. Meunier, Effective bulk and surface temperatures of the catalyst bed of FT-IR cells used for in-situ and operando studies, *Phys. Chem. Chem. Phys.* (2011). <https://doi.org/10.1016/j.corsci.2008.12.024>.
- [29] A. Travert, C. Fernandez, *SpectroChemPy* (Version 0.1), Zenodo. (2020). <http://doi.org/10.5281/zenodo.3823841>.
- [30] [www.spectrochempy.fr](http://www.spectrochempy.fr), (n.d.).

- [31] A. de Juan, J. Jaumot, R. Tauler, Multivariate Curve Resolution (MCR). Solving the mixture analysis problem, *Anal. Methods*. 6 (2014) 4964–4976.  
<https://doi.org/10.1039/C4AY00571F>.
- [32] F. Vilmin, I. Bottero, A. Travert, N. Malicki, F. Gaboriaud, A. Trivella, F. Thibault-Starzyk, Reactivity of bis[3-(triethoxysilyl)propyl] tetrasulfide (TESPT) silane coupling agent over hydrated silica: Operando IR spectroscopy and chemometrics study, *J. Phys. Chem. C*. 118 (2014) 4056–4071. <https://doi.org/10.1021/jp408600h>.
- [33] P. Grandvallet, P. de Jong, H. Mooiweer, A.G.T.G. Kortbeek, B. Kraushaar, Process for the conversion of a feedstock comprising linear olefins, EP 0 501 577 A1, 1992.
- [34] H. Hu, M. Ke, K. Zhang, Q. Liu, P. Yu, Y. Liu, C. Li, W. Liu, Designing ferrierite-based catalysts with improved properties for skeletal isomerization of n -butene to isobutene, *RSC Adv*. 7 (2017) 31535–31543. <https://doi.org/10.1039/c7ra04777k>.
- [35] H.H. Mooiweer, K.P. de Jong, B. Kraushaar-Czarnetzki, W.H.J. Stork, B.C.H. Krutzen, Skeletal isomerisation of olefins with the zeolite Ferrierite as catalyst., *Zeolites Relat. Microporous Mater. State Art*. 84 (1994) 2327–2334. [https://doi.org/10.1016/S0167-2991\(08\)63797-0](https://doi.org/10.1016/S0167-2991(08)63797-0).
- [36] J. Houzvicka, S. Hansildaar, J.G. Nienhuis, V. Ponec, The role of deposits in butene isomerisation, 176 (1999) 83–89.
- [37] B. de Menorval, P. Ayrault, N.S. Gnep, M. Guisnet, Mechanism of n-butene skeletal isomerization over HFER zeolites: a new proposal, *J. Catal*. 230 (2005) 38–51.  
<https://doi.org/10.1016/j.jcat.2004.09.021>.

- [38] P.J. Grobet, H. Geerts, J.A. Martens, P.A. Jacobs, Correct determination of aluminium in Y zeolites by magic angle spinning NMR spectroscopy, *J. Chem. Soc., Chem. Commun.* (1987) 1688–1690. <https://doi.org/10.1039/C39870001688>.
- [39] S. Bordiga, C. Lamberti, F. Bonino, A. Travert, Probing zeolites by vibrational spectroscopies, *Chem. Soc. Rev.* (2015).
- [40] T. Terlouw, J.-P. Gilson, Catalyst composition, EP0458378B1, 1994.
- [41] M.A. Makarova, A.E. Wilson, B.J. Van Liemt, C.M.A.M. Mesters, A.W. De Winter, C. Williams, Quantification of Bronsted acidity in mordenites, *J. Catal.* 172 (1997) 170–177. <https://doi.org/10.1006/jcat.1997.1849>.
- [42] P. Pissis, D. Daoukaki-diamanti, Dielectric Studies of Molecular Hydrated Mobility in Hydrated Zeolites, *J. Phys. Chem. Solids.* 54 (1993) 701–709. [https://doi.org/10.1016/0022-3697\(93\)90130-J](https://doi.org/10.1016/0022-3697(93)90130-J).
- [43] P. Andy, N.S. Gnep, M. Guisnet, E. Benazzi, C. Travers, Skeletal Isomerization of n-Butenes II. Composition, Mode of Formation, and Influence of Coke Deposits on the Reaction Mechanism, *J. Catal.* 173 (1998) 322–332. <https://doi.org/10.1006/jcat.1997.1945>.
- [44] C. Paze, B. Sazak, A. Zecchina, J. Dwyer, FTIR and UV-Vis Spectroscopic Study of Interaction of 1-Butene on H-Ferrierite Zeolite, *J. Phys. Chem. B.* 103 (1999) 9978–9986. <https://doi.org/10.1021/jp992117j>.
- [45] V.L. Zholobenko, D.B. Lukyanov, J. Dwyer, W.J. Smith, Ferrierite and SUZ-4 Zeolite: Characterization of Acid Sites, *J. Phys. Chem. B.* 5647 (1998) 2715–2721.

<https://doi.org/10.1021/jp973340o>.

- [46] I. Castellanos, O. Marie, An operando FT-IR study of the NO<sub>x</sub> SCR over Co-HFER and Fe-HFER using acetylene as a reducing agent, *Catal. Today*. 283 (2017) 54–65.  
<https://doi.org/10.1016/j.cattod.2016.02.034>.
- [47] T. Armaroli, M. Bevilacqua, M. Trombetta, J. Ramirez, G. Busca, An FT-IR study of the adsorption of aromatic hydrocarbons and of 2,6-lutidine on H-FER and H-ZSM-5 zeolites, *Appl. Catal.* 220 (2001) 181–190. [https://doi.org/10.1016/S0926-860X\(01\)00720-7](https://doi.org/10.1016/S0926-860X(01)00720-7).